Geomechanics and Engineering, *Vol. 28, No. 5 (2022) 505-520*
https://doi.org/10.12989/gae.2022.28.5.505

Shear behavior of geotextile-encased gravel columns in silty sand-Experimental and SVM modeling

Reza Dinarvand and Alireza Ardakani*

Department of Civil Engineering, Imam Khomeini International University, Qazvin, Iran

(Received August 28, 2021, Revised January 18, 2022, Accepted January 21, 2022)

Abstract. In recent years, geotextile-encased gravel columns (usually called stone columns) have become a popular method to increasing soil shear strength, decreasing the settlement, acceleration of the rate of consolidation, reducing the liquefaction potential and increasing the bearing capacity of foundations. The behavior of improved loose base-soil with gravel columns under shear loading and the shear stress-horizontal displacement curves got from large scale direct shear test are of great importance in understanding the performance of this method. In the present study, by performing 36 large-scale direct shear tests on sandy base-soil with different fine-content of zero to 30% in both not improved and improved with gravel columns, the effect of the presence of gravel columns in the loose soils were investigated. The results were used to predict the shear stress-horizontal displacement curve of these samples using support vector machines (SVM). Variables such as the non-plastic fine content of base-soil (FC), the area replacement ratio of the gravel column (Arr), the geotextile encasement and the normal stress on the sample were effective factors in the shear stress-horizontal displacement curve of the samples. The training and testing data of the model showed higher power of SVM compared to multilayer perceptron (MLP) neural network in predicting shear stress-horizontal displacement curve. After ensuring the accuracy of the model evaluation, by introducing different samples to the model, the effect of different variables on the maximum shear stress of the samples was investigated. The results showed that by adding a gravel column and increasing the Arr, the friction angle (ϕ) and cohesion (c) of the samples increase. This increase is less in base-soil with more FC, and in a proportion of the same Arr, with increasing FC, internal friction angle and cohesion decreases.

Keywords: geotextile; gravel columns; shear strength; silty-sand; support vector machines

1. Introduction

Gravel columns (GCs) or granular piles (or stone column) are among the economically and environmentally methods in improving clays, silt, loose silty-sands and sands, and soft soil deposits with low shear strength (Barksdale and Bachus 1983, Malekpoor and Poorebrahim 2014, Deb and Majee 2014). Treated soils by gravel columns have higher stiffness and strength than untreated soils (Murugesan and Rajagopal 2010). Improvement of soft clay by gravel or stone columns leads to an increase in vertical bearing capacity and a decrease in the settlement and an increase in the rate of consolidation (Bergado *et al.* 1990, Hughes *et al.* 1975, Gniel and Bouazza 2009, Gniel and Bouazza 2010, Araujo *et al.* 2009, Ghazavi and Afshar 2013, Hosseinpour *et al.* 2014, Zhang and Zhao 2015, Hong *et al.* 2016, Ardakani *et al.* 2018). In addition, the use of gravel columns reduces the liquefaction potential of sandy soil (Asgari *et al.* 2013). The overpressure of the pore water and the shear expansion of the loose soils are reduced by the installation of gravel columns and the drainage rate is increased (Adalier *et al.* 2003, Ashford *et al.* 2000). By encasing the stone columns by geotextile, the post-cyclic capacity of the gravel columns increases and the total settlement of the base-soil decreases (Yoo and Abbas 2020).

In 2019, Das and Deb conducted a series of three-dimensional experiments and numerical modeling to investigate the response of gravel columns to a fine-grained embankment loading. They concluded that by increasing the amount of embankment fines; it increases the pore water pressure and thus increases the time of the final consolidation meeting (Das and Deb 2019). In 2021, Aghili *et al.* studied the effect of granular column on cyclic shear resistance of clay, by performing 42 large-scale cyclic direct shear test. They showed that the use of granular column, increasing the diameter of column and increasing the relative density of the column aggregates improved the cyclic shear resistance of clay (Aghili *et al.* 2021).

Also, the shear bearing capacity of loose deposits is increased by gravel and stone columns. This issue is due to friction and locking between the grains of the gravel column (Naeini and Gholampour 2015). In addition, the stability of deep-seated failure of slopes located on loose soils increases due to use of gravel columns (Zhang *et al.* 2014). The use of an encasement around the stone column, which results in greater enclosure and more shear resistance mobilization, resolves the above mentioned problems. The use of geotextile as an encasement in loose soils improved by stone columns can prevent the lateral expansion of the column. Furthermore, some researchers have investigated the effect of geogrid-encased granular columns (Sivakumar

*Corresponding author, Associate Professor
E-mail: a.ardakani@eng.ikiu.ac.ir

ISSN: 2005-307X (Print), 2092-6219 (Online)

et al. 2004, Malarvizhi and Ilamparuthi 2007, Gniel and Bouazza 2010, Murugesan and Rajagopal 2010, Choobbasti and Pichka 2012, Zhou *et al.* 2019).

The resistance of the ground improved when encased granular columns were used. These have been studied by means of experiments, finite element models, and analytical methods (Yoo 2015, Pulko and Logar 2017, Hong *et al.* 2017, Cengiz and Guler 2018, Zhou *et al.* 2019, Zhang *et al.* 2020, Yu *et al.* 2020, Yoo and Abbas 2020, Lajevardi and Enami 2021, Sadr *et al.* 2022). The acceleration of the consolidation process increased and the settlement reduced using geotextile encased columns (Hong *et al.* 2016, Miranda *et al.* 2017). Moreover, the results of triaxial tests conducted by Miranda and Da Costa (2016) showed the improvement achieved when the stone column is encased with the geotextiles. Furthermore, the ESC reduced more lateral deformation of saturated sand strata, compared to the SC (Tang *et al.* 2015).

Several researchers have investigated the behavior of geotextile-encased gravel and stone columns (EGCs and ESCs) under vertical loading (Maheshwari and Khatri 2012, Dash and Bora 2013, Hosseinpour *et al.* 2014, Yoo *et al.* 2014, Zhang and Zhao 2015, Demir and Sarici 2017, Li *et al.* 2020), but there are not too many investigations about lateral loading on encased gravel and stone columns. A number of researchers have studied the behavior of ordinary stone columns under lateral loading in different methods (Han *et al.* 2004, Abusharar and Han 2011, Zhang *et al.* 2014, Dinarvand and Ardakani, 2017, Chen *et al.* 2020). Murugesan and Rajagopal (2008) examined the shear behavior of OGC and EGC in soft clay soils. They observed significant improvement in the shear strength of the columns as a result of the encasement. Chen *et al.* (2015) conducted a number of physical experiments and three-dimensional numerical modeling to investigate the behavior of embankments based on soft soil improved by encased stone columns, which showed that the GESCs failed under bending. Furthermore, in 2016, Mohapatra *et al.* showed that the shear bearing capacity of sandy bases increases by the installation of gravel columns, and this increase is greater in gravel columns encased with geotextiles (Mohapatra *et al.* 2016). In 2017, Mohapatra and Rajagopal, using 3D numerical modeling, showed that by installing encased gravel and stone columns, besides increasing the slope stability and reducing vertical and horizontal deformation, the possibility of deep-seated failure of slope is also reduced (Mohapatra *et al.* 2017).

In 2018, Naeini and Gholampour conducted a series of laboratory tests to investigate the effect of stone columns on the shear capacity of improved clay soils. The results of their research showed that by adding a stone column, the direct shear curve of the samples, like dense sandy soils, has a peak. It also increases the friction angle of the specimens by adding a stone column (Naeini and Gholampour 2018).

In 2019, Hajiazizi and Nasiri studied the behavior of stone columns in the stability of sandy slopes. Their results showed that the best place to install a gravel column is in the middle of the slope. Also, the bearing capacity of the slope and factor of safety (FOS) of slope stability increases with the installation of a gravel or stone column (Hajiazizi and Nasiri 2019).

In civil and geotechnical engineering, various methods such as numerical and laboratory modeling are used to study the behavior of structures and soil (Khorshidi *et al.* 2014, Cengiz and Guler 2018, Zhou *et al.* 2019, Shafigh *et al.* 2021). In recent years, the use of soft computing methods to model complex civil and geotechnical engineering problems has widely increased (Shahin, 2010). These methods include artificial neural networks (ANN) and support vector machines and etc.. (Lee and Lee 1996, Shahin and Indraratna 2006, Choobbasti *et al.* 2009, Tinoco *et al.* 2012, Alkayem *et al.* 2018, Soltangharaei *et al.* 2020). The advantage of soft computing methods is that they learn the pattern of phenomena directly from laboratory and experimental results, and the errors in the laboratory and the experimental data have little effect on the network.

Wood *et al.* (2005) used an artificial neural network to predict error in triaxial experiments with flexible boundaries (Wood *et al.* 2005). Najjar and Huang (2007) predicted stress-strain behavior of Georgia clay soil by recursive neural network (Najjar and Huang 2007). Lee and Hee (2008) modeled the nonlinear elastic behavior of lime-stabilized soils in triaxial shear strength experiments using neural networks (He and Li 2008). Tarawneh (2017) used artificial neural networks to predict the amount of N60 based on the results of the cone penetration test. The results showed that artificial neural networks with a hidden layer and six neurons in the hidden layer and sigmoid activation function can well predict the value of N60 (Tarawneh 2017). Motaleb Nejad *et al.* (2018) used artificial neural networks to predict shear wave velocities in different soils. The results showed that the neural network with two hidden layers and each layer of six neurons has the best performance in predicting shear wave velocity (Motalleb Nejad *et al.* 2018).

Rashidian and Hassanlorad also studied the stress-strain behavior of carbonate sands in both non-cemented and cemented states using artificial neural networks based on genetic algorithm. Their results showed that the stress-strain behavior of carbonate sands is well predictable using genetic algorithms based on genetic algorithms (Rashidian and Hassanlourad 2013).

In 2017, Das and Dey developed the bearing capacity of stone columns in soft clay by developing 16 artificial neural network models and 4 different learning algorithms. They used laboratory data and the results of two-dimensional numerical analysis to teach and evaluate the model. The results of their research showed that the BR algorithm is more accurate than other learning algorithms. Also, the sensitivity analysis of the model showed that the friction angle of the gravel column materials has the most, and the column length has the least effect on the bearing capacity of the stone columns (Das and Dey 2017). Also Das and Dey in 2017 showed that Neuro-fuzzy systems are highly accurate in predicting the bearing capacity of stone columns (Das and Dey 2017). Ahmad Dar and Yousuf Shah in 2020, using data got from a series of three-dimensional finite element analysis and the development of a multilayer regression model, the FOS of embankments based on They examined the stone column. Their research showed that by encasing the gravel column with geotextile, increasing the

angle of friction of the stone column material, and the cohesion of the base soil, the FOS increases. Also, the neural network with a hidden layer and 20 neurons per layer can estimate the slope stability FOS with a correlation coefficient of 0.9958 (Ahmad Dar and Yousuf Shah 2020).

Support vector machines are one of the soft computing methods that have shown high capability in predicting geotechnical properties of soils. Deswal and Pal (2008), Liu *et al.* (2011), Zhang *et al.* (2012) and Kordjazi *et al.* (2014), are examples of application of this method in geotechnical problems. The advantage of this method compared to other soft computing methods is that by minimizing the structural risk, along with reducing the model error, its generalizability increases (Ardakani and Kouhestani 2017).

In 2017, Debnath and Dey used the support vector regression (SVR) to investigate the bearing capacity of geogrid-reinforced stone columns. To develop the SVR model, they used the data got from large-scale experiments. The results of their studies showed the SVR model with ERBF kernel function has the best performance with high generalizability and low error in predicting the bearing capacity of geogrid-reinforced stone columns (Debnath and Dey 2017). Also in 2017, Aljanbi *et al.* examined the behavior of stone columns in highway embankments. They used the SVM method with the RBF kernel function to predict the subsidence of embankments on gravel columns (Aljanbi *et al.* 2017). In 2018, Das and Dey investigated the bearing capacity of stone columns in soft clay with the help of support vector machines. They conclude the SVM model is more accurate in predicting the bearing capacity of stone columns than the ANN model. Also, the load-bearing capacity of the stone column and the base soil is affected by the non-drained adhesion of the base soil, the friction angle of the gravel column materials, the distance to column diameter ratio, and the length of the stone columns, respectively (Das and Dey 2018).

It was observed that in the technical literature, there are many studies on the performance of encased stone and gravel columns in improving soil behavior under different loading, such as static and dynamic loading and as normal and shear loads in different soils. Use of encased stone and gravel columns lead to a decrease in the settlement of clay soils, increase the rate of pore water disappearance in fine-grained soils, reduce the liquefaction potential of saturated sandy soils, increase the stability of slopes, increase the shear strength of soils and increase the bearing capacity of foundations. However, no special study has been done on the behavior of these columns in silty sand soils under lateral loading and the application of SVM method in predicting the shear stress-horizontal displacement curve.

In the present study, 36 large-scale direct shear test were performed to investigate the shear behavior of sand base-soil with different fine-grained material improved by gravel columns. Then, with the help of support vector machines and artificial neural networks, a model is presented to predict the shear behavior of base-soil treated by gravel columns. Factors such as the amount of silt grain in the sand base, normal stress on the sample, geotextile encasement and also the area replacement ratio of gravel columns were considered as input to the problem.

2. Support vector machines (SVM)

In 1992, based on statistical theories, Vapnik proposed a method called support vector machines for classification and regression problems. Initially, this statistical theory was a linear classification, which was later introduced as a nonlinear classification using kernel functions. In 1996, regression vector machines based on regression were published by Vapnik et al. (Vapnik and Cortes 1995, Smola and Scholkopf 2004).

In SVMs, to minimize the model error, the structural risk minimization method is used. In this method, unlike the experimental risk minimization method which is used in artificial neural networks. The model error minimization and its generalizability maximization are performed simultaneously (Dibike *et al.* 2001).

In SVM, the regression problem is solved using a loss function and accepting the minimum error ε and estimating regression using a set of linear or nonlinear functions. To solve the regression problem on a set of data as $\{(x_1,y_1),\ldots,(x_n,y_n) \in R_m , y \in R\}$ linear equation of number 1 is formed.

$$f(x)=\langle w.x\rangle + b \quad (1)$$

In this regard; n: Number of samples, x: Input vector, y: Output vector, b: bias, w: weight vector.

The loss function with area ε is also defined as follows.

$$L_\varepsilon(y) = |y - f_x|_\varepsilon = \begin{cases} 0, & |y - f_x| \le \varepsilon \\ |y - f_f| - \varepsilon, & \text{otherwise} \end{cases} \quad (2)$$

In this equation, Lε(y) is a function of losses, and ε is a fixed and positive value.

The optimal function control parameters (weight "w" and bias "b") are obtained by solving the following optimization problem.

Minimize

$$\Phi(w,\xi^*,\xi) = \frac{\|w\|^2}{2} + C(\sum \xi^* + \sum \xi)$$

Subject to:

$$y_i - ((w.x_i) + b) \le \varepsilon + \xi_i$$
$$((w.x_i) + b) - y_i \le \varepsilon + \xi_i \qquad i = 1,2,\ldots,n$$
$$\xi_i, \xi_i^* \ge 0$$

In the above equations, $\|w\|^2$ is the norm of weight factors, C is the adjustment parameter, ξ_i و ξ_i^* are the slack variables shown in Fig. 1.

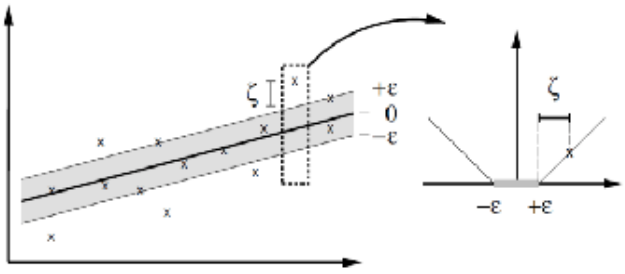

Fig. 1 Vapnik loss function and slack variables (Debnath and Dey 2017)

The above optimization problem can be converted to a lagrange function as follows.

$$L(\alpha^*, \alpha) = -\varepsilon \sum_{i=1}^{n}(\alpha_i^* + \alpha_i) + \sum_{i=1}^{n} y_i(\alpha_i^* + \alpha_i) - \frac{1}{2}\sum_{i=1}^{n}\sum_{j=1}^{n}(\alpha_i^* - \alpha_i)(\alpha_i^* + \alpha_i)(x_i . x_j) \quad (3)$$

In the above equation, $L(\alpha^*, \alpha)$ is lagrange function and α^* and α are Lagrange coefficients. The above function is maximized under the following constraints.

$$\sum \alpha_i^* = \sum \alpha_i$$
$$0 \le \alpha_i^* \le C \quad (4)$$
$$0 \le \alpha_i \le C$$

The final answer, by obtaining α^* and α coefficients, will be as follows.

$$w_0 = \sum_{\text{Support vectors}} (\alpha_i^* - \alpha_i)x_i \quad (5)$$

$$b_0 = -\frac{1}{2} w_0 . [x_r + x_s] \quad (6)$$

$$f(x) = \sum_{\text{Support vectors}} (\alpha_i^* - \alpha_i)(x_i . x) + b_0 \quad (7)$$

In the above equations, w_0 and b_0 are optimal weight and bias values, x_r and x_s are two support vectors.

Support vectors are data whose corresponding lagrange coefficients are non-zero. Geometrically, this data, which has a prediction error greater than ±ε controls the number of support vectors. In this case, due to the use of QP (Quadratic Programming) method, the possibility of achieving the general extreme and preventing falling into the local extreme is definite (Samui 2008).

In the support vector machine model, C constant and ε constant are introduced by the user. C parameter, which regulates the balance between experimental risk minimization and model generalization maximization, can be between zero and infinite. Large values of C parameter reduce the training data error and in contrast reduce the scalability of the index, while small values of this parameter reduce the generalizability by accepting higher errors.

The ε parameter, which affects the status of the support and working vectors of the model, can accept values from zero to infinity. Very large values of this parameter increase the generalizability of the model by increasing the allowable error. On the other hand, for very small values of ε, due to the very small error of the model, with increasing support vectors, there is a possibility that the model becomes more training.

With the help of kernel functions, it is possible to turn the linear regression problem in non-linear vector machines into nonlinear regression (Cristianini and Shawe 2000). There are various kernel functions in support vector machines, including 'polynomial functions', 'radial basis functions', and 'Pearson function' in geotechnics. By using kernel functions, equations can be written as follows.

$$w_0 . x = \sum_{\text{Support Vectors}} (\alpha_i^* - \alpha_i)K(x_i, x) \quad (8)$$

$$b_0 = -\frac{1}{2} \sum_{\substack{\text{Support} \\ \text{Vectors}}} (\alpha_i^* - \alpha_i)[K(x_r, x_i) + K(x_s, x_i)] \quad (9)$$

In the above equations, K (xi, x) is a kernel function.

3. Model training and evaluation

In the present study, the SVM model was trained and tested using Weka software. The polynomial kernel function was used to extend the nonlinear model. The polynomial kernel function is as follows.

$$K(x, x_i) = (\langle x, x_i \rangle + 1)^d \quad (10)$$

In the above equation, d is the power of the function that is introduced by the user. Figure 2 summarizes the development steps of the SVM-model.

4. Data used in model construction

In order to achieve an efficient model for predicting the shear capacity of improved base-soil with gravel columns, it is necessary to identify the factors affecting the behavior of samples under direct shear test. These factors include information about the materials used and the conditions of the test. The data used in the present study result from 36 large-scale direct shear test performed by the researchers.

A large-scale direct shear box has been used to investigate the shear stress-horizontal displacement of sand+different silt content improved by gravel columns. The box had a plane size of 30 cm × 30 cm and a depth of 17 cm. The real height of sample inside the shear box was 15 cm for each test. The experiments continued to reach 40mm horizontal displacement. Though the diameter of the gravel column in each test is small compared with the real diameter of a full-scale gravel column or stone column, the tests have been performed at normal stress levels typical of the real embankment (Mohapatra *et al.* 2016).

Sand with different FC, (0–30 percent), was used to prepare the sandy base soil. GP (poorly-graded gravel) was used as gravel columns material. The grain size distribution curve of coarse grain (gravel and sand) and fine grain (silt) material was performed according to ASTM D422 & ASTM D422-63 standards respectively.

The maximum dry density were obtained according to the ASTM D4253 standard shaking table and minimum dry density were obtained according to the ASTM D4254 standard. In the case of base soil with 20 percent and 30 percent fine content, the maximum dry density were obtained according to the ASTM D1557 standard.

UPVC pipes with two different diameter—55 & 110 mm—were used to construct GCs to investigate the effect of increase in the Arr of the GCs. Fig. 3 shows the grain size distribution of base soil and gravel column material. The ratio of diameter of column to maximum aggregate size was nearly 18 in the case of 110-mm-diameter column, and 10 in the case of 55-mm-diameter of column. According to Fox (2011) and Stoeber (2012), a value of 10 and more is satisfactory for this ratio. In addition, the dimensions of the

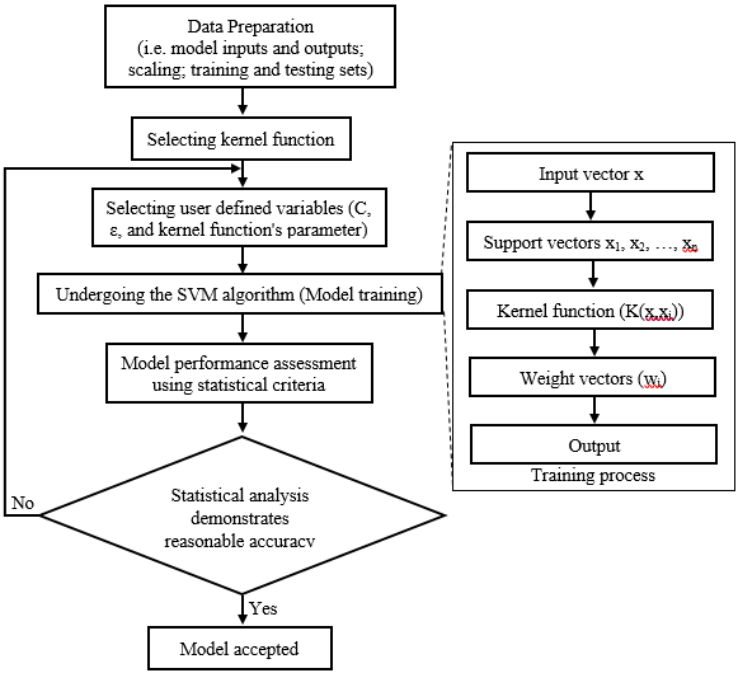

Fig. 2 Summary of steps involved in the process of model development using the SVM (Kordjazi *et al*. 2014)

model and grain size are appropriate for the effect of grain size on the interaction as well as the shear band patterns (Garnier *et al*. 2007).

The mechanical and physical characteristics of the sand base and the gravel column are given in Tables 1 and 2, respectively. Also, the grain size characteristics of the materials used to make the sand base and gravel column and non-woven geotextile are given in Table 3. The sand base was made in a loose state with a Dr (Relative density) of 30% and the gravel column in a dense condition with a Dr of 80%**.**

To make the sandy base, the sample was prepared in five layers with gentle blows until it reached a density of 30%. To construction of gravel columns, PVC tubes whose inner diameter was equal to the diameter of the gravel column were used. To compact the gravel column materials, the materials were poured in five layers.

Table 1 mechanical properties of base-soil

Fine content (%)	e_{max}	e_{min}	G_s
0	0.87	0.57	2.67
10	0.85	0.46	2.67
20	0.83	0.37	2.67
30	0.83	0.32	2.67

Table 2 mechanical properties of gravel column material

Properties	Value
γ_d (gr/cm3)	*1.69*
γ_{dmin} (gr/cm3)	*1.54*
γ_{dmax} (gr/cm3)	*1.73*
D_r (*%*)	*80*

Table 3 grading properties of base-soil, gravel column material and mechanical properties of geotextile encasement

Properties	Gravel Column	Fine content (%)			
		30	20	10	0
D10 (mm)	*2.20*	*0.02*	*0.03*	*0.04*	*0.15*
D30 (mm)	*3.90*	*0.04*	*0.06*	*0.16*	*0.18*
D60 (mm)	*8.52*	*0.20*	*0.21*	*0.21*	*0.22*
Cu	*3.86*	*8.70*	*6.83*	*4.77*	*1.47*
Cc	*0.81*	*4.90*	*3.66*	*2.77*	*0.98*
Soil classification	*GP*	*SM*	*SM*	*SP-SM*	*SP*
Geotextile	*Ultimate tensile stress*	*39 kN/m*			
	Thickness	*3.3 mm*			
	Permeability	*5.5x10-3 m/s*			

Each layer received 50 blows using a rod 10 mm in diameter and 20 cm high. After making the samples, which was done completely dry, the sample was submerged. After complete saturation of the nucleus, normal stress applied to the sample. At the end of the vertical session under normal load, shear displacement applied to the specimens at a speed of 1 mm / min. The experiment continued until a displacement of 40 mm. Fig. 4 shows the plane of sample with EGC and the test program is shown in Table 4.

The experimental results showed an increase in the strength and stiffness of the base soil because of the installation of gravel columns. The gravel column provides more shear capacity due to the higher shear strength because of friction and inter-locking between its grains. GC1 is a column with a Arr = 2.64% and GC2 is a column with a Arr = 10.55% (Fig. 5 (a)).

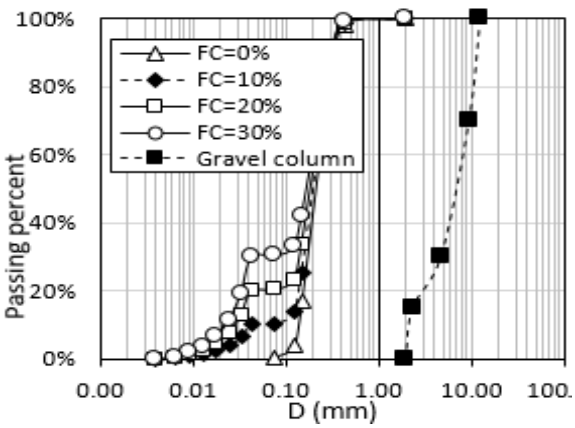

Fig. 3 Grain size distribution

Fig. 4 Plane view of a single gravel column with geotextile encasement

Table 4 Experimental program in direct shear test

Influencing factors	Parameter Range
Fine content (%)	0
	10
	20
	30
Normal stress (kPa)	10
	30
	60
	120
Area replacement ratio (%)	0
	2.64
	10.56
Tensile strength of geotextile (kN/m)	0
	39

Improving the behavior of the base soil is not the same in different fine-grained bases, and with increasing the amount of base fine-grained, the effect of gravel columns decreases. Also, with increasing the ratio of the replacement level of the gravel column, the maximum resistance increases (Fig. 5 (b)).

In ordinary type of gravel column, the GC was completely sheared, but in the case of the EGCs, the geotextile encasement showed higher shear strength because of the confinement (Mohapatra *et al*. 2016). The strain-softening behavior observed in the case of GC was converted to strain-hardening (in the case of EGC) due to the encasement effect. At first, the shear deformation is

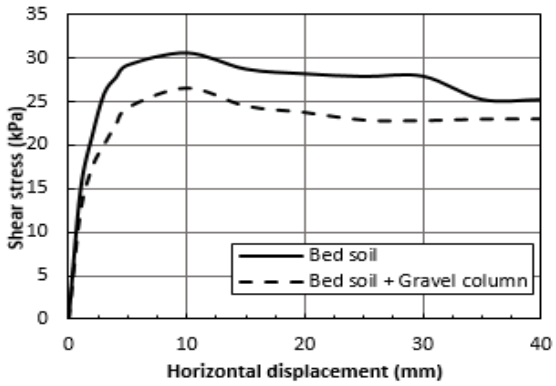

(a) FC = 0%

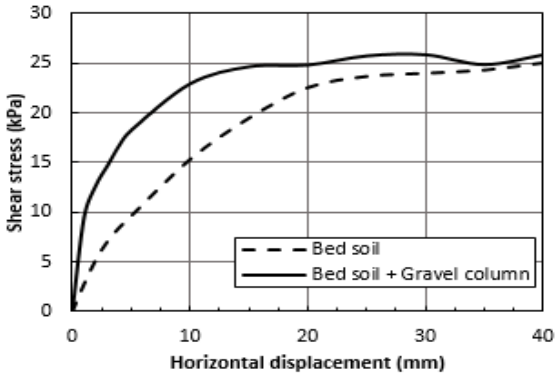

(b) FC = 30%

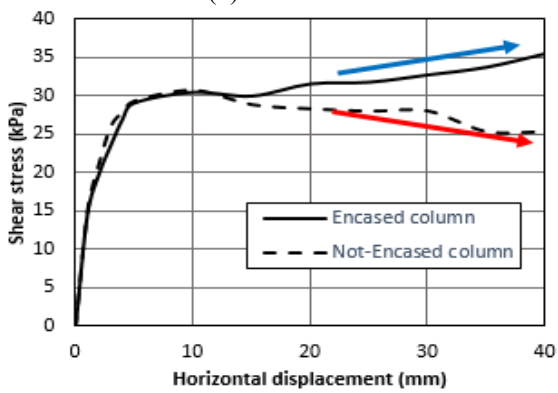

(c) FC = 0%

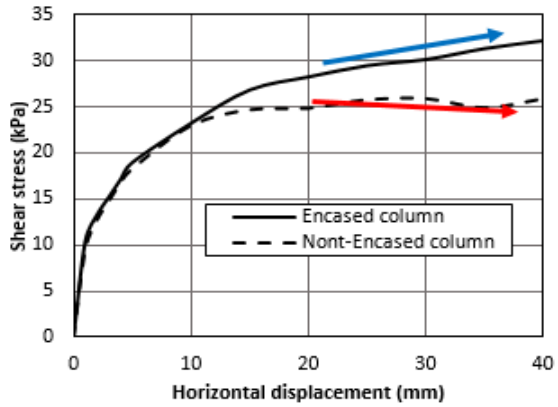

(d) FC = 30%

Fig. 5 Shear stress-horizontal displacement

merely the mobilization of the shear strength of the gravel column material, which is stiffer than sandy material around it. After shear strength is mobilized, strain-hardening behavior was observed. Chen *et al*. (2015) pointed out that the bending failure is the main failure mode in the case of geotextile encased columns under lateral loading (Fig 5(c) and (d)). Increase in residual shear strength due to EGCs can be describe by the apparent cohesion which appears due to the effect of confinement of geotextile. The geotextile encasement increases the shear resistance of gravel columns due to mobilization of tensile stresses in the encasement layer (Mohapatra *et al*. 2016).

The residual shear strength of base soil, GCs, and EGCs at different fine contents of base soil are listed in Table 5. In the samples with ordinary gravel columns, the residual shear strength is almost the same, but in the samples with encased gravel columns, the residual shear strength decreased by the increase in silt content due to increase in the e_i and reduction in geotextile-sand interaction (Naeini and Gholampoor 2014).

Fig. 6 shows the residual shear strength of base soil improved by ordinary gravel columns and encased gravel columns normalized by residual shear strength of not-improved base soil. The normalized residual shear strength decreased by increasing silt contents of base soil from 10 percent to 5 percent for ordinary gravel columns and from 55 percent to 30 percent for encased gravel column.

Besides the area replacement ratio of column and the amount of fine content of base, normal stress on the samples is the factor affecting the behavior of the soil under direct shear testing. According to the above, the input data includes the amount of substrate fineness (FC), the ratio of column replacement level and normal stress, and the output is the shear stress. Also, since the horizontal axis of the curve got from the direct shear test is horizontal displacement, another input is the horizontal displacement of the specimens. Table 6 shows the statistical characteristics of the input and output data of the problem.

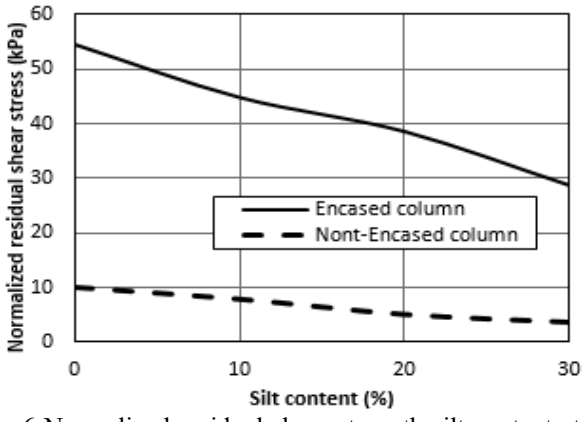

Fig. 6 Normalized residual shear strength-silt content at 30 kPa normal stress

Table 5 Residual shear strength of sand base soil, GCs and EGCs (kPa)

Fine Content	Base Soil	GC	EGC
0 percent	22.95	25.29	35.45
10 percent	23.89	25.78	34.57
20 percent	24.62	25.85	34.09
30 percent	25.02	25.90	32.19

Table 6 statistical parameters of inputs and output of model

Statistical parameters	FC (%)	Normal stress (kPa)	Arr (%)	Tensile strength of encasement	Horizontal Displacement (mm)	Shear stress (kPa)
Max	*30*	*120*	*10.6*	*35*	*40*	*95*
Min	*0*	*10*	*0*	*0*	*0*	*0*
Mean	*14.9*	*33.9*	*4.1*	*7.2*	*14.6*	*23.5*
STD	*11.8*	*26*	*4.6*	*14.3*	*13.5*	*18.2*

5. Model performance evaluation indicators

In order to evaluate the accuracy of the model got from the statistical indicators such as correlation coefficient (CC), mean square error (MSE), root mean square error (RMSE), Mean absolute value of error percentage (MAPE), and mean absolute deviation (MAD) were used. The values of the mentioned indicators are obtained using the following equations

$$CC = \frac{\sum_{i=1}^{n}[(s_i - \bar{s}_i)(c_i - \bar{c}_i)]}{\sqrt{\sum_{i=1}^{n}(s_i - \bar{s}_i)^2 (c_i - \bar{c}_i)^2}} \quad (11)$$

$$MSE = \frac{\sum_{i=1}^{n} E_i^2}{n} \quad (12)$$

$$RMSE = (MSE)^{0.5} \quad (13)$$

$$MAPE = \frac{\sum_{i=1}^{n}|E_i|}{\sum_{i=1}^{n} s_i} \quad (14)$$

$$MAD = \frac{\sum_{i=1}^{n}|E_i|}{n} \quad (15)$$

$$E_i = (s_i - c_i) \quad (16)$$

In the above equations, $\bar{c}_i$ is the mean variable observational value, $\bar{s}_i$ is the average value calculated by the model, c_i is the actual observational value of the variable, s_i is the value of the variable calculated by the model and n is number of observational data.

6. Model used

In order to teach the model and achieve the optimal fit, which has both the least prediction error and the most generalizability, the trial and error method must be used. In

this way, by assigning different values to the parameters and comparing their effect on the correlation coefficient and RMSE, the appropriate values of the parameters are selected. 85% of the data was used for training and the remaining 15% were used for testing.

In the present study, to select the parameters c, d and e by trial and error, by assigning the values shown in Figs. 7-9, the most optimal value was got as follows.

c=2.5, e=0.005, d=20

Figs. 10 and 11 show the evaluation of the model got from the model for training and testing data, respectively. Table 7 shows the model performance results. According to the results, the model presented by the SVM-model has a high accuracy. Figs. 12 and 13 also show that the differences between the results of experiments and the predicted output from the model are very close. In Figs. 12 and 13, the 'Error' refers to the difference between the target shear stress and the output shear stress (Error = Target - Output).

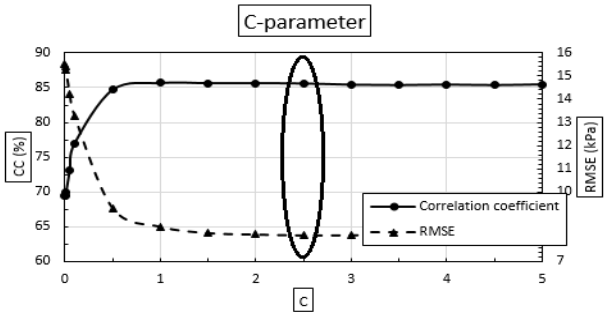

Fig. 7 Changes in correlation coefficient and root mean square error by changing the c parameter

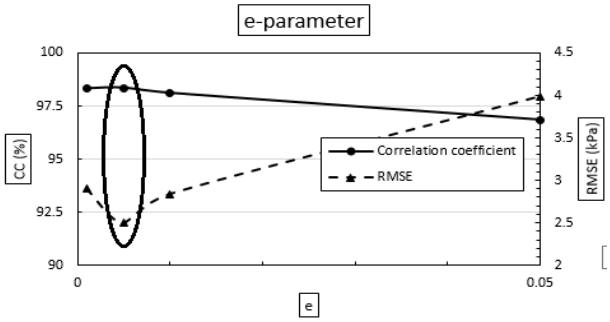

Fig. 8 Changes in correlation coefficient and root mean square error by changing the e parameter

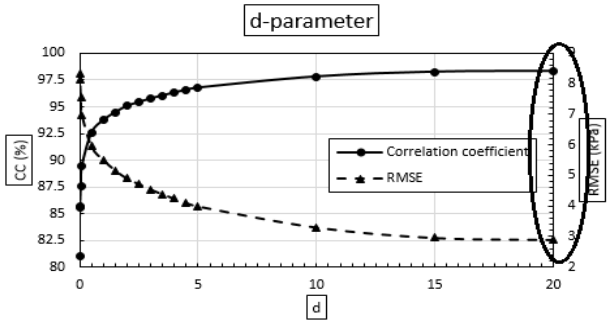

Fig. 9 Changes in correlation coefficient and root mean square error by changing the d parameter

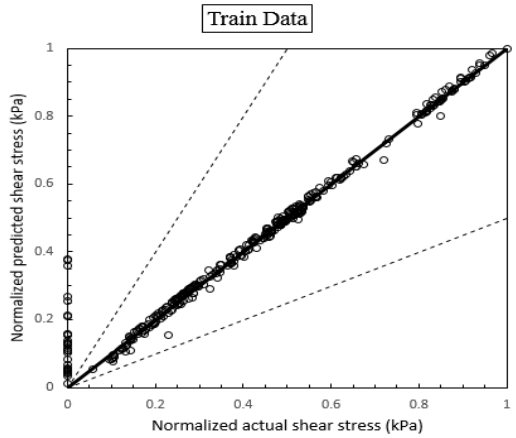

Fig. 10 Correlation between actual results and predicted results for training data (SVM model)

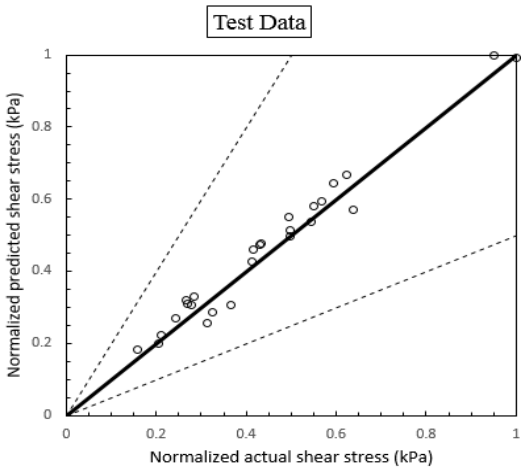

Fig. 11 Correlation between actual results and predicted results for testing data (SVM model)

Table 7 Performance evaluation indicators of SVM model

SVM	CC	RMSE (kPa)	MAPE	MAD (kPa)
Train	0.9814	2.46	5%	1.00
Test	0.9851	1.30	6%	1.69

For further comparison, the input data of the two experiments performed were introduced to the model, and the curve got from the model was compared with the experiments results. Figs. 14-20 show the shear stress-horizontal displacement curve got from the model and experiments results. As shown in the figure, the SVM model is able to accurately estimate the shear stress-horizontal displacement curve obtained from the direct shear test.

To comparison between the SVM model and the MLP-model, the training and testing data used in the SVM model were introduced to the MLP model. Figs. 21 and 22 show the correlation between the results obtained from the direct shear test and the results predicted by the MLP model. Table 8 also presents the statistical results of the accuracy of the MLP model. The comparison between the SVM model and the MLP model shows that the SVM model is more accurate.

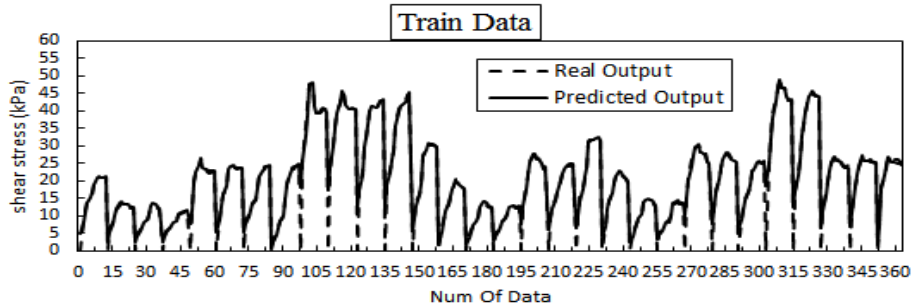

Fig. 12 Model error in the training phase

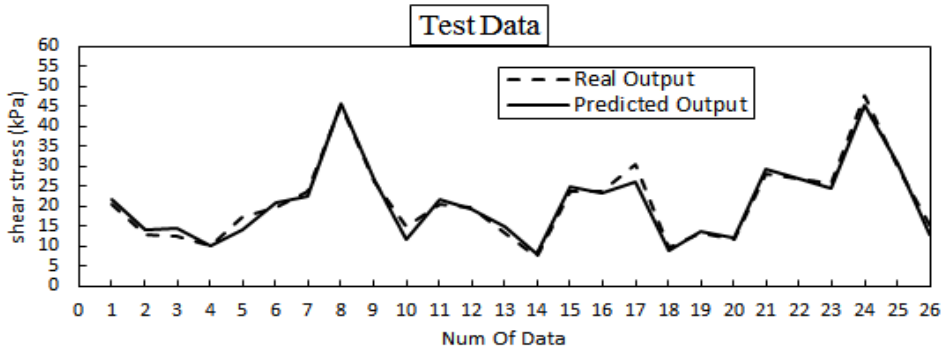

Fig. 13 Model error in the testing phase

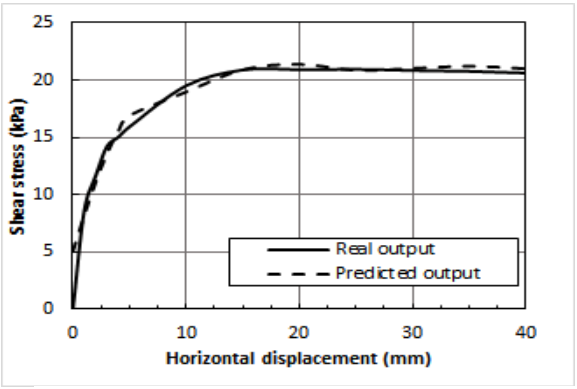

Fig. 14 Shear stress-horizontal displacement curve-real and predicted by SVM model FC = 0% at normal stress of 10 kPa

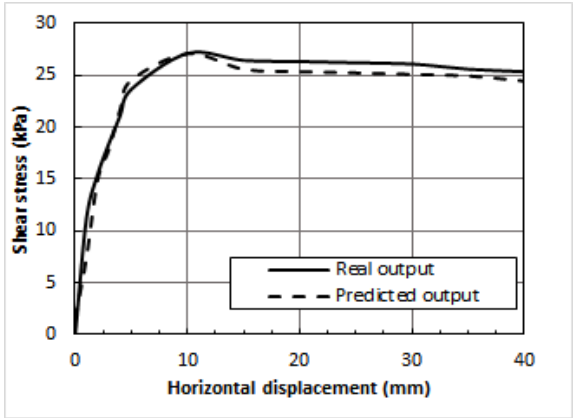

Fig. 15 Shear stress-horizontal displacement curve-real and predicted by SVM model FC = 20% improved by GC1 at a normal stress of 30 kPa

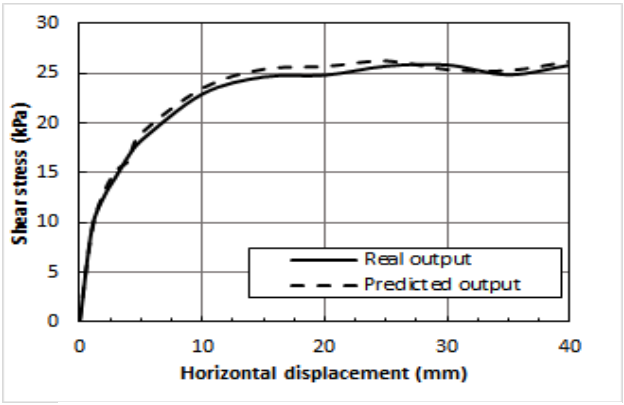

Fig. 16 Shear stress-horizontal displacement curve-real and predicted by SVM model FC = 30% improved by GC2 at a normal stress of 30 kPa

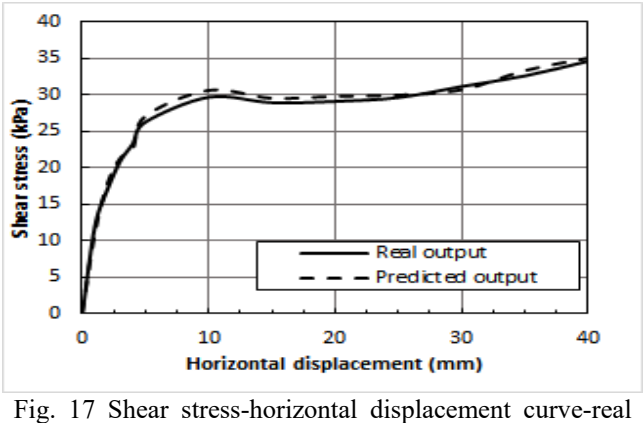

Fig. 17 Shear stress-horizontal displacement curve-real and predicted by SVM model FC = 10% improved by EGC2 at a normal stress of 30 kPa

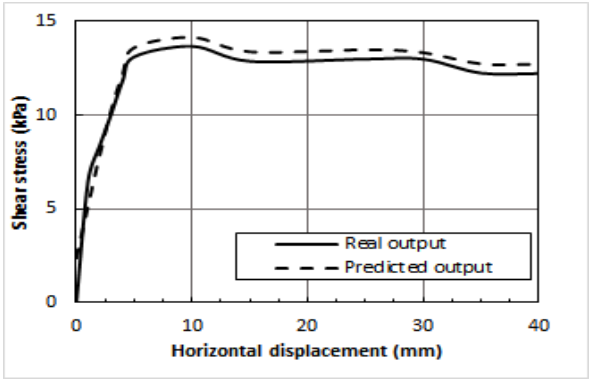

Fig. 18 Shear stress-horizontal displacement curve-real and predicted by SVM model FC = 10% at a normal stress of 10 kPa

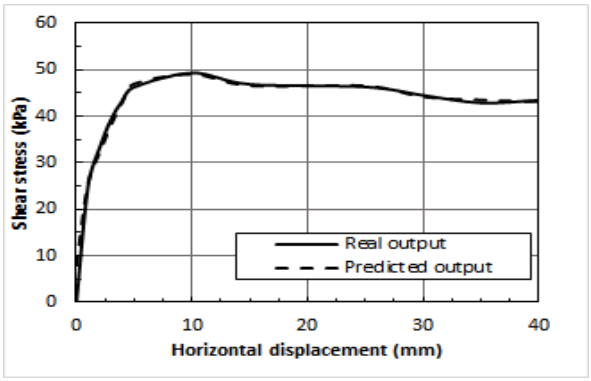

Fig. 19 Shear stress-horizontal displacement curve-real and predicted by SVM model FC = 0% improved by GC2 at a normal stress of 60 kPa

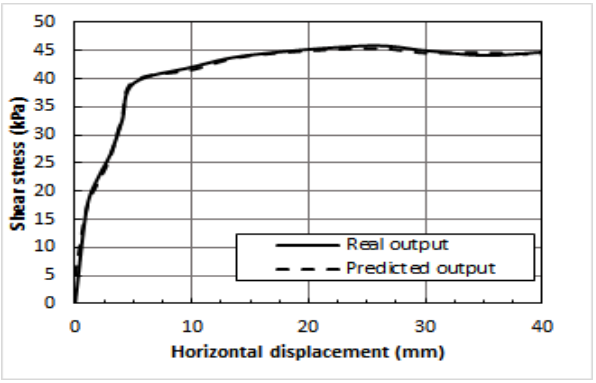

Fig. 20 Shear stress-horizontal displacement curve-real and predicted by SVM model FC = 30% improved by GC2 at a normal stress of 60 kPa

Table 8 Performance evaluation indicators of MLP model

MLP model	CC	RMSE (kPa)
Train data	0.9279	4.79
Test data	0.8855	4.85

7. Effect of variables input

To investigate the effect of inputs of the model, by changing the input parameters, shear stress- horizontal displacement diagrams for different conditions were obtained. The following results from changing the input parameters on the maximum shear stress of the models.

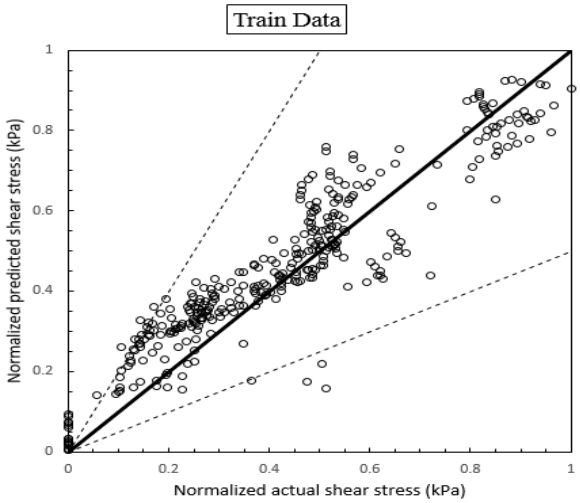

Fig. 21 Correlation between actual results and predicted results (MLP model) - Train Data

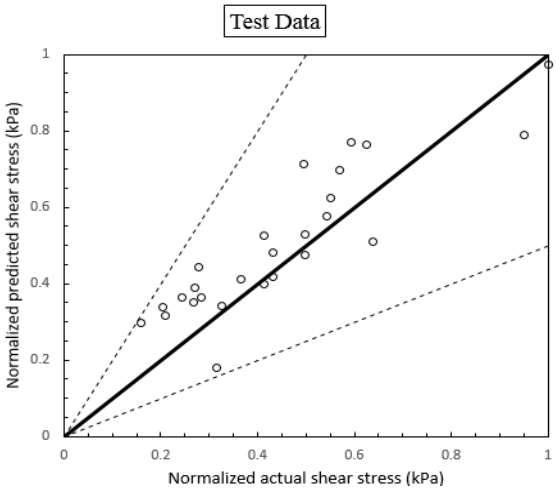

Fig. 22 Correlation between actual results and predicted results (MLP model) - Test Data

7.1 Effect of area replacement ratio (Arr)

The gravel column, which has a higher friction angle and compaction, mobilizes greater shear strength than untreated loose soil. As the Arr increases, the gravel column, acts at a higher shear strength level. Christoulas *et al.* (1997) pointed out that the shear resistance of the base soil improved with gravel columns can be estimated as follows

$$\tau_c A_c + \tau_s A_s = \tau A \quad (17)$$

Where τ_C and τ_S are the shear strengths of the gravel aggregate and base soil, respectively, Ac and As are the plane areas of the gravel columns and base soil, respectively.

In most cases, shear strength is much lower than theoretical estimate. Therefore, a correction factor (α) is

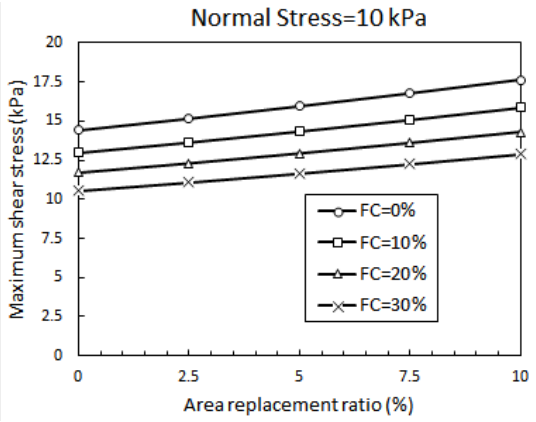

Fig. 23 Maximum shear stress– area replacement ratio - normal stress = 10 kPa

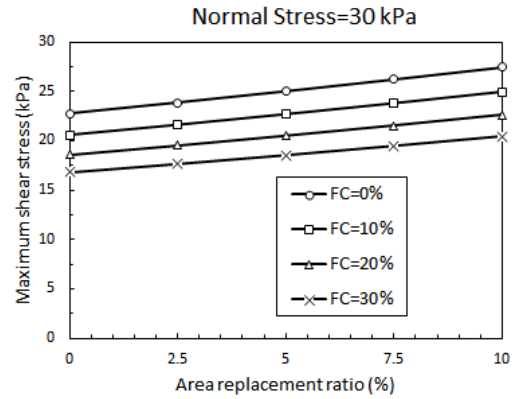

Fig. 24 Maximum shear stress– area replacement ratio - normal stress = 30 kPa

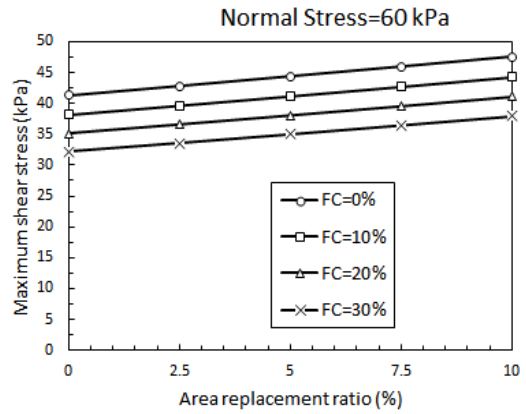

Fig. 25 Maximum shear stress– area replacement ratio - normal stress = 60 kPa

used to make a realization. By applying this correction factor, Eq. (18) is used as follows. Murugesan and Rajagopal (2008) reported this correction factor between 0.4 and 0.9 depending on the normal stresses on the sample.

$$\tau_c A_c + \alpha\tau_s A_s = \tau A \quad (18)$$

This could be due to the fact that the gravel columns may not have developed their full shear resistance due to insufficient confinement and shear resistance from the moving base soil mass (Murugesan and Rajagopal 2008).

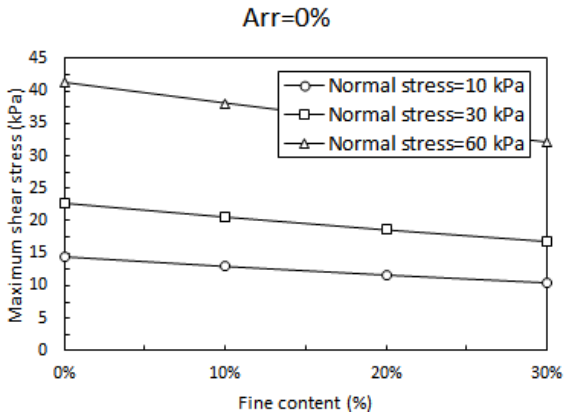

Fig. 26 Maximum shear stress -fine content Arr = 0%

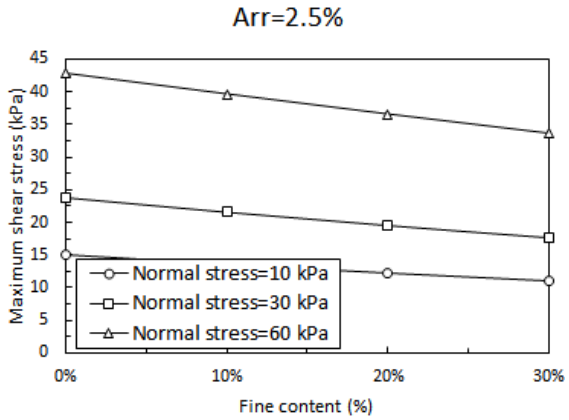

Fig. 27 Maximum shear stress -fine content Arr = 2.5%

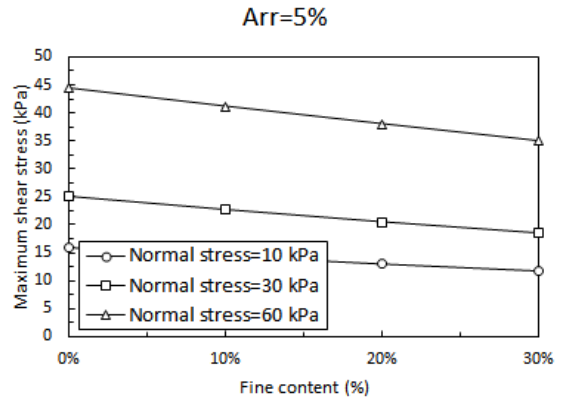

Fig. 28 Maximum shear stress -fine content Arr = 5%

According to Eqs. (17) and (18), as the A_c (Arr) increases, the shear strength of base soil+GC will increase. The effect of increasing the Arr on the maximum shear stress of the models is shown in the Figs. 23-25.

7.2 Effect of fine content (FC) of base-soil

Gravel columns do not have the same effect in different soils. By increasing the amount of fine-grained in base-soil, less shear strength is mobilized by the base soil + gravel column . In the case of FC=0%, because of the frictional capacity of the substrate soil, some of the shear displacement resistance is provided by the substrate soil.

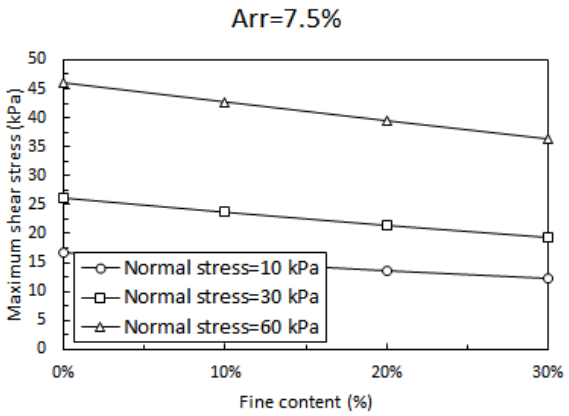

Fig. 29 Maximum shear stress -fine content Arr = 7.5%

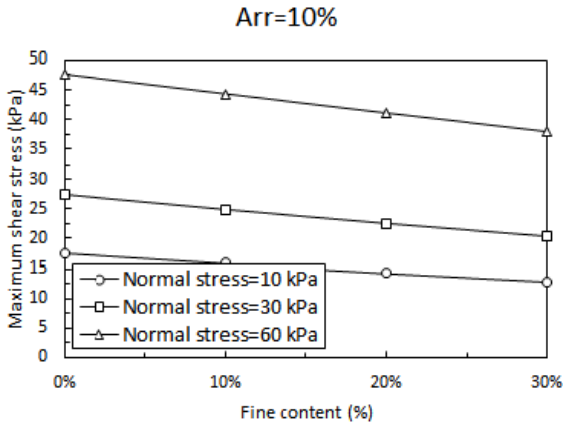

Fig. 30 Maximum shear stress -fine content Arr%10 =

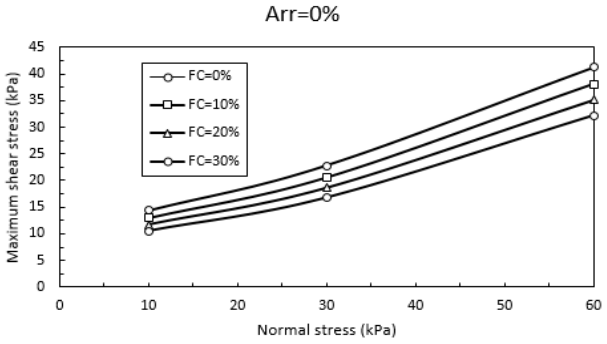

Fig. 31 Maximum shear stress -normal stress Arr%0 =

But with increasing the FC, the stiffness of the base soil decreases. This reduction in stiffness makes the shear displacement resistance more affected by the gravel column. The presence of fine particles in the pores of the gravel column reduces the frictional capacity of the gravel column. In Figs. 26-30, the diagram of changes in maximum shear stress against increasing the FC is shown.

7.3 Effect of normal stress

The SVM-models were analyzed at three different normal stresses of 10, 30 and 60 kPa. Increasing the normal stress causes the specimens to become more compact before horizontal displacement. Increasing the density and inter-

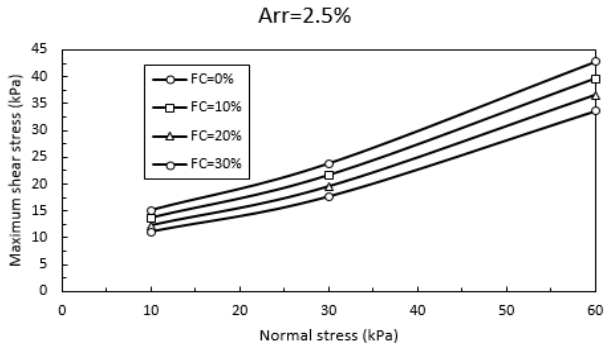

Fig. 32 Maximum shear stress - normal stress Arr%2.5=

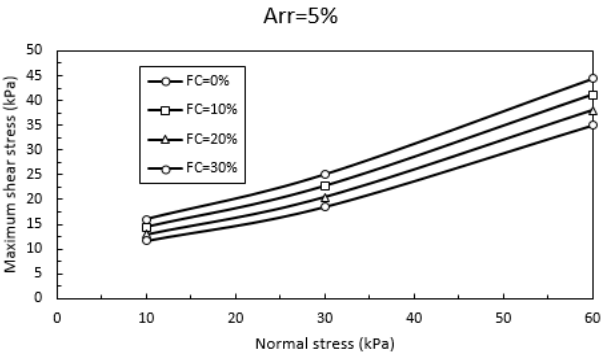

Fig. 33 Maximum shear stress - normal stress Arr = 5%

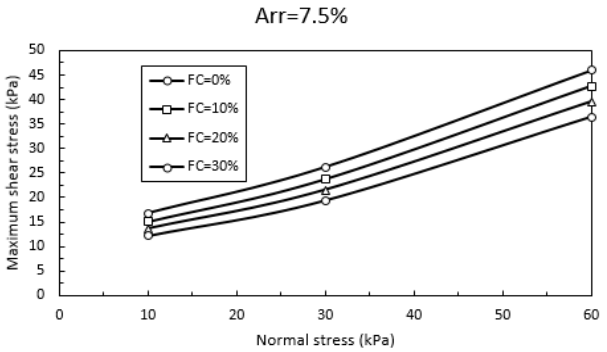

Fig. 34 Maximum shear stress - normal stress Arr = 7.5%

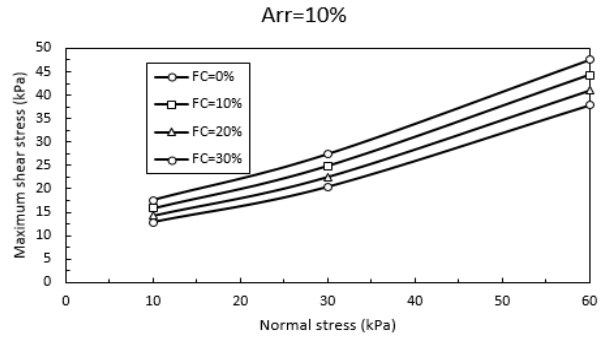

Fig. 35 Maximum shear stress - normal stress Arr = 10%

locking between the soil grains, leads to more shear strength mobilization. This effect is not the same in base-soil with different fines. As in base-soil with more fines, less resistance is observed. This is due to the nature of more fine-grained soils, which have lower friction angles than

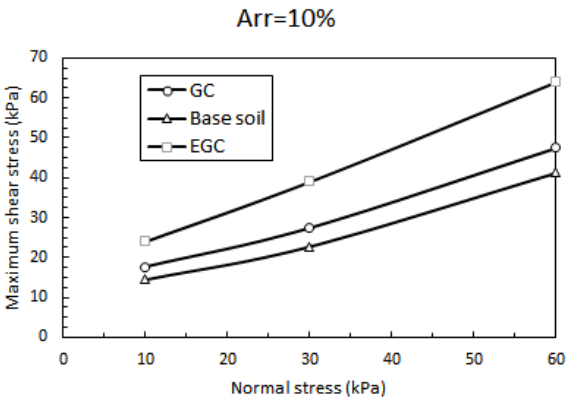

Fig. 36 Maximum shear stress - normal stress FC = 10% , Arr = 10

non-fine-grained soils. Figs. 31-35 show the maximum stress-normal shear strength diagram for different models with different gravel column replacement ratios. From these diagrams, two important parameters of cohesion and friction angle can be obtained.

7.4 Effect of geotextile encasement

The encasement of the column increases the radial stresses towards the inside of the column and maintains the density of gravel grains inside the column. Therefore, the material inside the column does not lose its frictional capacity after applying normal stress and during the shear displacement. In the Fig. 36 the residual shear stress against normal stress of base soil with ordinary gravel columns and encased gravel columns in base soil with FC=0% is drawn. As shown in this figure, for EGCSs type of column, the residual shear stress is more than the residual shear stress of GCs. In loose sand base soils, the effect of ordinary GCs is not significant, because of the low lateral confinement of surrounding sand soil and shear failure of gravel material of GCs.

8. Conclusions

In the present study, by conducting a series of large-scale direct shear tests on sandy base-soil with different fine content in both unimproved and improved with gravel columns, the effect of gravel column presence on shear strength of bases were investigated. Then support vector machines were used to predict the shear stress-horizontal displacement curve obtained from the experiments. Data from 36 large-scale direct shear tests were used to train and test the model. Comparing the results obtained from the model obtained from the SVM model and MLP model with the laboratory results, it was observed that:

- The shear resistance of loose base soil has been increased due to the installation of the gravel column. The increase in shear strength is because of the fact that the gravel column has greater relative density and friction angle than the surrounding soil. The results showed that the maximum shear stress increased between 4 percent and 16 percent in the case of ordinary GCs.
- In the geotextile-encased gravel columns samples, the residual strength has increased compared to ordinary gravel columns. Moreover, the failure mechanism of gravel column was changed from shear failure to bending failure because of the encasement. Furthermore, geotextile encasement increases the shear resistance of gravel columns due to mobilization of tensile stresses in the encasement layer. The results showed that the maximum shear stress increased between 26 percent and 54 percent in the case of EGCs.
- In the case of ordinary gravel column and encased gravel column, an increase in shear resistance was observed with an increase in the area replacement ratio of columns. The maximum shear stress increased by increasing the Arr of columns from 5 percent to 10 percent in the case of GCs and from 47 percent to 54 percent in the case of EGCs.
- In all tests and models, the stress and stiffness of the samples have declined due to increases in the fine content. The normalized maximum shear strength decreased by increasing silt content of sand base soil from 10 percent to 5 percent for GCs and from 55 percent to 30 percent for EGCs.
- The SVM model can predict laboratory results, with an index Statistics CC = 0.9821 and RMSE = 2.308. The model had acceptable performance for both training data, and test data.
- The SVM model has a better performance than MLP model to predict the shear stress-horizontal displacement curve of gravel columns.
- Also, by analyzing of the model output to input variables, it was found that with increasing the ratio of gravel column substitution surface, the cohesion and friction angle of the samples increases and the rate of increase, decreases by increase the fine content of base-soil.
- Geotechnical engineers can refer to the graphs presented in this paper to understand the effect of using gravel columns in soils with similar grading (sand with 0% to 30% silt) in improving the shear capacity of these soils, especially when they are placed at the downstream of a slope or floor of embankments. Also it can be seen the effect of encasing the columns under the shear load and increasing the shear capacity of gravel columns, especially in their ultimate strength. However, for practical use of these results, engineers must follow the rules of scaling. The presented results are applicable to an initial approximation.

References

Abusharar, S.W. and Han, J. (2011), "Two-dimensional deep-seated slope stability analysis of embankments over stone column-improved soft clay", *J. Eng. Geol.*, **120**(1-4), 103-110. https://doi.org/10.1016/j.enggeo.2011.04.002.

Adalier, K., Elgamal, A., Meneses, J. and Baez, J. (2003), "Stone

columns as liquefaction countermeasure in non-plastic silty soils", *Soil Dyn. Earthq. Eng*., **23**(7), 571-584. https://doi.org/10.1016/S0267-7261(03)00070-8.

Aghili. E., Hosseinpour, I., Jamshidi, R. and Ahmadi, H. (2021), "Behavior of granular column-improved clay under cyclic shear loading", *Transport Geotech.*, **31**, https://doi.org/10.1016/j.trgeo.2021.100654.

Aljanabi, Q.A., Chik, Z, Allawi, M.F., El-Shafie, A.H., Ahmed, A.N. and El-Shafie, A. (2017), "Support vector regression-based model for prediction of behavior Stone column parameters in soft clay under highway embankment", *Neural Comput. Appl*., https://doi.org/10.1007/s00521-016-2807-5**.**

Alkayem. N.F., Cao, M., Zhang, Y., Bayat, M. and Su, Z. (2018), "Structural damage detection using finite element model updating with evolutionary algorithms: a survey", *Neural Comput, Appl.*, **30**(2), 389-411. https://doi.org/10.1007/s00521-017-3284-1.

Alkhorshid, N.R., Araujo, L.S., Palmeira, E.M. and Zornberg, J.G. (2019), "Large-scale load capacity tests on a geosynthetic encased column", *Geotext. Geomembranes*., **47**(5), 632-641. https://doi.org/10.1016/j.geotexmem.2019.103458.

Andreou, P. and Papadopoulos, V. (2014), "Factors affecting the settlement estimation of Stone column reinforced soils", *Geotech. Geol. Eng*., **32**, 1175-1185. https://doi.org/10.1007/s10706-014-9788-x.

Ardakani, A., Gholampoor, N., Bayat, M. and Bayat, M. (2018), "Evaluation of monotonic and cyclic behavior of geotextile encased stone columns", *Struct. Eng. Mech*., **65**(1), 81-89. https://doi.org/10.12989/sem.2018.65.1.081.

Asgari, A., Oliaei, M. and Bagheri, M. (2013), "Numerical simulation of improvement of a liquefiable soil layer using Stone column and pile-pinning techniques", *Soil Dyn. Earthq. Eng*., **51**, 77-96. https://doi.org/10.1016/j.soildyn.2013.04.006.

Ashford, S.A., Rollins, K.M. and Baez, J.I. (2000), "Comparison of deep foundation performance in improved and non-improved ground using blast induced liquefaction", *Proc., Geo-Denver 2000, Soil Dynamics and Liquefaction. ASCE Geotech. Special Publ*., **23**, 20-34.

Barksdale, R.D. and Bachus, R.C. (1983), "Design and Construction of Stone Columns", *Report FHWA.RD-83.026. National Information Service, Springfield, Virginia.*

Basack, S., Indraratna, B., Rujikiatkamjorn, C. and Siahaan. F. (207), "Modeling the Stone column behavior in soft ground with special emphasis on lateral deformation", *J. Geotech. Geoenviron. Eng*., **143**(6), 04017016. https://doi.org/10.1061/(ASCE)GT.1943-5606.0001652.

Bergado, D.T., Singh, N., Sim, S.H., Panichayatum, B., Sampaco, C.L. and Balasubramaniam, A.S. (1990), "Improvement of soft Bangkok clay using vertical geotextile band drains compared with granular piles", *Geotext. Geomembranes*, **9**(3), 203-231. https://doi.org/10.1016/0266-1144(90)90054-G.

Cengiz, C. and Güler, E. (2018), "Seismic behavior of geosynthetic encased columns and ordinary stone columns" *Geotext. Geomembranes*, **46**(1), 40-51. https://doi.org/10.1016/j.geotexmem.2017.10.001.

Cengiz, C., Kilic, I.E. and Güler, E. (2019), "On the shear failure mode of granular column embaseded unit cells subjected to static and cyclic shear loads", *Geotext. Geomembranes*, **47**(2), 193-202. https://doi.org/10.1016/j.geotexmem.2018.12.011.

Chakraborty, A. and Goswami, D. (2017), "Prediction of slope stability using multiple linear regression (MLR) and artificial neural network (ANN)", *Arab. J. Geosci*., **10**, 385. https://doi.org/10.1007/s12517-017-3167-x.

Chen, J.F., Li, L.Y., Xue, J.F. and Feng, S.Z. (2015), "Failure mechanism of geosynthetic encased gravel columns in soft soils under embankment", *Geotext. Geomembranes*, **43**(5), 424-431. https://doi.org/10.1016/j.geotexmem.2015.04.016.

Chen, J.F., Li, L.Y., Zhang, Z., Zhang, X., Xu, C., Rajesh, S. and Feng, Z. S. (2020) "Centrifuge modeling of geosynthetic-encased stone column-supported embankment over soft clay" *Geotext. Geomembranes*, https://doi.org/10.1016/j.geotexmem.2020.10.021**.**

Choobbasti, A.J. and Pichka, H. (2012). "Improvement of soft clay using installation of geosynthetic-encased stone columns: numerical study" *Arab. J. Geosci*., https://doi.org/10.1007/s12517-012-0735-y.

Christoulas, S., Giannaros, C. and Tsiambaos, G. (1997), "Stabilization of embankment foundations by using stone columns", *Geotech. Geolo. Eng*., **15**, 247-258. https://doi.org/10.1007/BF00880828.

Dar, L.A. and Yousuf Shah, M. (2020), "Deep-seated slope stability analysis and development of simplistic FOS Evaluation models for stone column-supported embankments", *T. Infrastruct. Geotechnology*, https://doi.org/10.1007/s40515-020-00134-7.

Das, A.K. and Deb, K. (2016), "Modeling of stone column-supported embankment under axi-symmetric condition", *Geotech. Geol. Eng*., https://doi.org/10.1007/s10706-016-0136-1.

Das, A.K. and Deb, K. (2019), "Response of stone column-improved ground under c-/ϕ soil embankment", *Soils Found*., **59**, 617-632. https://doi.org/10.1016/j.sandf.2019.01.003.

Das, A.K. and Deb, K. (2018), "Experimental and 3D numerical study on time dependent behavior of Stone column-supported embankments", *Int. J. Geomech., ASCE*., **18**(4), 1-16. https://doi.org/10.1061/(ASCE)GM.1943-5622.0001110.

Das, M. and Dey, A.K. (2017), "Determination of bearing capacity of stone column with application of neuro-fuzzy system", *KSCE J. Civ. Eng*., 1-7. https://doi.org/10.1007/s12205-017-1497-6**.**

Das, M. and Dey, A.K. (2017), "Prediction of bearing capacity of stone columns placed in soft clay using ANN model", *Geotech. Geol. Eng*., https://doi.org/10.1007/s10706-017-0436-0.

Das, M. and Dey, A.K. (2018), "Prediction of bearing capacity of stone columns placed in soft clay using SVR model", *Arab. J. Sci. Eng*., https://doi.org/10.1007/s13369-018-3513-7.

Dash, S.K. and Bora, M.C. (2013), "Influence of geosynthetic encasement on the performance of gravel columns floating in soft clay", *Can. Geotech. J.*, **50**(7), 754-765. https://doi.org/10.1139/cgj-2012-0437.

Deb, K. and Majee, A. (2014), "Probability-based design charts for stone column-improved ground", *Geomech. Eng*., **7**(5), 539-552. https://doi.org/10.12989/gae.2014.7.5.539.

Debnath, P. and Dey, A.K. (2018), "Prediction of bearing capacity of geogrid-reinforced stone columns using support vector regression", *Int. J. Geomech*., **18**(2), 04017147. https://doi.org/10.1061/(ASCE)GM.1943-5622.0001067.

Demir, A. and Sarici, T. (2017), "Bearing capacity of footing supported by geogrid encased stone columns on soft soil", *Geomech. Eng.,* **12**(3), 417-439. https://doi.org/10.12989/gae.2017.12.3.417.

Dinavand, R. and Ardakani, A. (2019), "Behavior of geosynthetic-encased granular column in silty sand soil by direct shear test", *Amirkabir. J. Civ. Eng*., **50**(5), 961-972. https://doi.org/10.22060/ceej.2017.12979.5308**.**

Emami, M. and Yasrebi, S. (2014), "Application of artificial neural networks in interpretation of pressuremeter test results", *Modares. Civ. Eng. J*., **14**(20), 11-25. http://mcej.modares.ac.ir/article-16-5107-fa.html.

Etezad, M., Hanna, A.M. and Ayadat, T. (2015), "Bearing capacity of a group of Stone columns in soft soil", *Int. J. Geomech. ASCE*., **15**(2), https://doi.org/10.1061/(ASCE)GM.1943-5622.0000393.

Fox, Z.P. (2011), "Critical State, Dilatancy and Particle Breakage

of Mine Waste Rock", Master's thesis. Colorado State University, Fort Collins, USA.

Garnier, J., Gaudin, C., Springman, S.M., Culligan, P.J., Goodings, D., Konig, D., Kutter, B., Phillips, R., Randolph, M.F. and Thorel, L. (2007), "Catalogue of scaling laws and similitude questions in geotechnical centrifuge modelling", *Int. J. Phys. Model. Geotech.*, **7**(3), 1-24. https://doi.org/10.1680/ijpmg.2007.070301.

Gniel, J. and Bouazza, A. (2010), "Construction of geogrid encased Stone columns: a new proposal based on laboratory testing", *Geotext. Geomembranes*, **28**(1), 108-118. https://doi.org/10.1016/j.geotexmem.2009.12.012.

Hagan, M.T. and Menhaj, M.B. (1994), "Training feedforward networks with the marquartdt algorithm", *IEEE T. Neural Networ.*, **5**(6), 989-992.

Han, J., Sheth, A.R., Porbaha, A. and Shen, S.L. (2004), "Numerical analysis of embankment stability over deep mixed foundations. Geotechnical Engineering for Transportation Projects", *Proceedings of Geo-Trans 2004, 126 II. Geotechnical Special Publication,* Los Angeles, CA, United States.

He, S. and Li, J. (2008), "Modeling nonlinear elastic behavior of reinforced soil using artificial neural networks", *Appl. Soft Comput.*, **9**(3), 954-961. https://doi.org/10.1016/j.asoc.2008.11.013.

Hong, Y.S., Wu, C.S. and Yu, S.Y. (2016), "Model tests on geotextile-encased granular columns under 1-g and undrained conditions" *Geotext. Geomembranes*, **44**, 13-27. https://doi.org/10.1016/j.geotexmem.2015.06.006.

Hong, Y.S., Wu, C.S., Kou, C.M. and Chang, C.H. (2017), "A numerical analysis of a fully penetrated encased granular column", *Geotext. Geomembranes*, **45**(5), 391-405. https://doi.org/10.1016/j.geotexmem.2017.05.002.

Hosseinpour, I., Riccio, M. and Almeida, M.S.S. (2014), "Numerical evolution of a granular column reinforced by geosynthetics using encasement and laminated disks", *Geotext. Geomembranes*, **42**(4), 363-373. https://doi.org/10.1016/j.geotexmem.2014.06.002.

Hughes, J.M.O., Withers, N.J. and Greenwood, D.A. (1975), "A field trial of the reinforcing effect of a granular column in soil", *Geotechniq.*, **25**(1), 31-44.

Karkush, M. and Jabba, A. (2019), "Improvement of soft soil using linear distributed floating stone column under foundation subjected to static and cyclic loading", *Civ. Eng. J.*, **5**(3), 702-711.

Khorshidi, N., Ansari, M. and Bayat, M. (2014), "An investigation of water magnetization and its influence on some concrete specificities like fluidity and compressive strength", *Comput. Conceret*, **13**(5), 649-657. https://doi.org/10.12989/cac.2014.13.5.649.

Lajevardi. S.H. and Enami. S. (2021), "Small scale behavior of stone columns encased by tires", *Geomech. Eng.*, **25**(5), 429-438. https://doi.org/10.12989/gae.2021.25.5.429.

Lee, I.M. and Lee, J.H. (1996), "Prediction of pile bearing capacity using artificial neural networks", *Comput. Geotech.*, **18**(3), 189-200. https://doi.org/10.1016/0266-352X(95)00027-8.

Li., L.Y., Rajesh, S. and Chen., J.F. (2020), "Centrifuge model tests on the deformation behavior of geosynthetic-encased stone column supported embankment under undrained condition", *Geotext. Geomembranes*, https://doi.org/10.1016/j.geotexmem.2020.11.003**.**

Malarvizhi, S.N. and Ilamparuthi, K. (2007), "Comparative behaviour of encased stone column and conventional stone column", *Soils Found.,* **47**(5), 873-885. https://doi.org/10.3208/sandf.47.873.

Malekpoor. M. and Poorebrahim. G. (2014), "Comparative study on the behavior of lime-soil columns and other types of stone columns", *Geomech. Eng.,* **7**(2), 133-148. https://doi.org/10.12989/gae.2014.7.2.133.

Mashenwari, P. and Khatri, S. (2019), "Influence of inclusion of geosynthetic layer on response of combined footings on stone column reinforced earth beds", *Geomech. Eng.,* **4**(4), 263-279. https://doi.org/10.12989/gae.2012.4.4.263.

Miranda, M. and Da Costa, A. (2016), "Laboratory analysis of encased stone columns", *Geotext. Geomembranes*, **44**, 269-277. https://doi.org/10.1016/j.geotexmem.2015.12.001.

Miranda, M., Da Costa, A., Castro, J. and Sagaseta, C. (2017), "Influence of geotextile encasement on the behaviour of stone columns: Laboratory study", *Geotext. Geomembranes*, **45**, 14-22. https://doi.org/10.1016/j.geotexmem.2016.08.004.

Mohanty, P. and Samanta M. (2015), "Experimental and numerical studies on response of the Stone column in layered soil", *Int. J. Geosynth. Ground Eng.*, https://doi.org/10.1007/s40891-015-0029-z.

Mohapatra, S.R., Rajagopal, K. and Sharma, J. (2016), "Direct shear tests on geosynthetic-encased granular columns", *Geotext. Geomembranes*, **44**(3), 396-405. https://doi.org/10.1016/j.geotexmem.2016.01.002.

Motalleb Nejad, M., Momeni, M.S. and Manahiloh, K.N. (2018), "Shear wave velocity and soil type microzonation using neural networks and geographic information system", *Soil Dyn. Earthq. Eng.*, **104**, 54-63. https://doi.org/10.1016/j.soildyn.2017.10.001.

Murugesan, M. and Rajagopal, K. (2010), "Studies on the behaviour of single and group of geosynthetic encased stone columns", *J. Geotech. Geoenviron. Eng.*, **136**(1), 129-139. https://doi.org/10.1061/(ASCE)GT.1943-5606.0000187.

Murugesan, S. and Rajagopal, K. (2008), "Shear load tests on granular columns with and without geosynthetic encasement", *Geotech. Test. J.*, **32**(1), 35-44.

Murugesan, S. and Rajagopal, K. (2010), "Studies on the behavior of single and group of geosynthetic encasemed granular columns", *J. Geotec. Geoenviron. Eng.*, **136**(1), 129-139. https://doi.org/10.1061/(ASCE)GT.1943-5606.0000187.

Naeini, S.A. and Gholampoor, N. (2014), "Cyclic behaviour of dry silty sand reinforced with a geotextile", *Geotext. Geomembranes*, **42**(6), 611-619. https://doi.org/10.1016/j.geotexmem.2014.10.0

Naeini, S.A. and Gholampoor, N. (2018), "Effect of geotextile encasement on the shear strength behavior of stone column-treated wet clays", *Indian Geotech. J.* https://doi.org/10.1007/s40098-018-0329-z.

Najjar, Y.M. and Huang, C. (2007), "Simulating the stress–strain behavior of Georgia kaolin via recurrent neuronet approach", *Comput. Geotech.*, **34**(5), 346-361. https://doi.org/10.1016/j.compgeo.2007.06.006.

Nasiri, M. and Hajiazizi, M. (2019), "An experimental and numerical investigation of reinforced slope using geotextile encased Stone column", *Int. J. Geotech. Eng.*, https://doi.org/10.1080/19386362.2019.1651029.

Pulko, B. and Logar, J. (2017), "Fully coupled solution for the consolidation of poroelastic soil around geosynthetic encased stone columns", *Geotext. Geomembranes*, **45**(6), 616-626. https://doi.org/10.1016/j.geotexmem.2017.08.003.

Rashidian, V. and Hassanlourad, M. (2013), "Predicting the shear behavior of cemented and uncemented carbonate sands using a genetic algorithm-based artificial neural network", *Geotech. Geol. Eng.*, **2**, 1-18. https://doi.org/10.1007/s10706-013-9646-2.

Sadr, A., Kaliakin, V.N., Htaf. N. and Manahiloh, K.N. (2022), "Numerical study of soilbag columns and comparison to encased soil columns in loose sand", *Comput. Geotech.*, **142**, https://doi.org/10.1016/j.compgeo.2021.104588.

Samui, P. (2013), "Liquefaction prediction using support vector machine model based on cone penetration data", *Front Struct. Civ. Eng.*, **7**(1), 72-82. https://doi.org/10.1007/s11709-013-

0185-y.
Shafigh, A., Ahmadi, H.R. and Bayat, M. (2014), "Seismic investigation of cyclic pushover method for regular reinforced concrete bridge", *Struct. Eng. Mech.*, **78**(1), 41-52 https://doi.org/10.12989/sem.2021.78.1.041.
Shahin, M.A. (2010), "Intelligent computing for modeling axial capacity of pile foundations", *Soil Dyn. Earthq. Eng*., **47**(2), 230-243. https://doi.org/10.1139/T09-094.
Sitton, J.D., Zeinali, Y. and Zeinali, B.A. (2017), "Rapid soil classification using artificial neural networks for use in constructing compressed earth blocks", *Constr. Build. Mater*., **138**, 214-221. https://doi.org/10.1016/j.conbuildmat.2017.02.006.
Sivakumar, V., McKelvey, J., Graham, J. and Hughes, D. (2004), "Triaxial test on model sand columns in clay", *Can. Geotech. J.,* **41**(2), 299-312. https://doi.org/10.1139/t03-097.
Smola, A.J. and Schölkopf, B. (2004), "A tutorial on support vector regression. Statistics and computing", *Statist. Comput*., **14**(3), 199-222. https://doi.org/10.1023/B:STCO.0000035301.49549.88.
Soltangharaei. V., Anay, R., Assi, L., Bayat, M., Rose, J.R., Ziehl. P. (2020), "Analyzing acoustic emission data to identify cracking modes in cement paste using an artificial neural network", *Constr. Build. Mater.*, 267, https://doi.org/10.1016/j.conbuildmat.2020.121047.
Stoeber, J.N. (2012), "Effects of Maximum Particle Size and Sample Scaling on the Mechanical Behavior of Mine Waste Rock; a Critical State Approach", Master's Thesis. Colorado State University, Fort Collins, USA.
Tabchouche, S., Mellas, M. and Bouassida, M. (2017), "On settlement prediction of soft clay reinforced by a group of Stone columns", *Innov. Infrastruct. Solut*., **2**(1), https://doi.org/10.1007/s41062-016-0049-0.
Tang, L., Zhang, X. and Ling, X. (2015), "Numerical simulation of centrifuge experiments on liquefaction mitigation of silty soils using stone columns", *KSCE J. Civ. Eng.*, **20**(2), 631-638. https://doi.org/10.1007/s12205-015-0363-7.
Tarawneh, B. (2017), "Predicting standard penetration test N-value from cone penetration test data using artificial neural networks", *Geosci. Front*., **8**(1), 199-204. https://doi.org/10.1016/j.gsf.2016.02.003.
Vapnik, V. N., Golowich, S.E. and Smola, A. (1996), "Support Vector Method for Function Approximation, Regression Estimation, and Signal Processing, Advances in Neural Information Processing Systems", *Morgan Kaufmann, San Mateo*.
Wood, D.M., Dihoru, L., Sadek, T. and Lings. M. (2005), "A neural network for error prediction in a true triaxial apparatus with flexible boundaries", *Comput. Geotech*., **32**(2), 59-71. https://doi.org/10.1016/j.compgeo.2005.01.003.
Yoo, C. (2015), "Settlement behavior of embankment on geosynthetic-encased stone column installed soft ground. A numerical investigation", *Geotext. Geomembranes*, **43**, 484-492. https://doi.org/10.1016/j.geotexmem.2015.07.014.
Yoo, C. and Abbas, Q. (2020), "Laboratory investigation of the behavior of a geosynthetic encased Stone column in sand under cyclic loading", *Geotext. Geomembranes,* https://doi.org/10.1016/j.geotexmem.2020.02.002.
Yoo, W., Kim, B. and Cho, W. (2014), "Model Test Study on the Behavior of Geotextile Encased Sand Pile in Soft Clay Ground" *KSCE J. Civ. Eng.*, **19**(3), 592-601. https://doi.org/10.1007/s12205-012-0473-4.
Yu. Y., Wang. Z. and Sun. H.Y. (2020), "Optimal design of stone columns reinforced soft clay foundation considering design robustness", *Geomech. Eng.*, **22**(4), 305-318. https://doi.org/10.12989/gae.2020.22.4.305.
Zhang, L. and Zhao, M. (2015), "Deformation analysis of geotextile-encased gravel columns", *ASCE Int. J. Geomech.*, **15**(3), 04014053.
Zhang, L., Xu, Z. and Zhou, S. (2020), "Vertical cyclic loading response of geosynthetic-encased stone column in soft clay" *Geotext. Geomembranes*, https://doi.org/10.1016/j.geotexmem.2020.07.006**.**
Zhang, Z., Han, J. and Ye, G. (2014), "Numerical investigation on factors for deep-seated slope stability of stone column-supported embankments over soft clay", *J. Eng. Geol.*, **168**, 104-113. https://doi.org/10.1016/j.enggeo.2013.11.004.
Zhou, Y. and Kong, G. (2019), "Deformation analysis of geosynthetic-encased stone column–supported embankment considering radial bulging", *Int. J. Geomech*., **19**(6), 04019057. https://doi.org/10.1061/(ASCE)GM.1943-5622.0001426.
Zhou, Y., Kong, G., Peng, H., Li, C., and Qin, H. (2019), "Visualization of bulging development of geosynthetic-encased stone column", *Geomech. Eng. J.*, **18**(3), 329-337 http://dx.doi.org/10.12989/gae.2019.18.3.329.

CC